Computers in Biology and Medicine 122 (2020) 103835

Contents lists available at ScienceDirect

Computers in Biology and Medicine

journal homepage: www.elsevier.com/locate/compbiomed

Capabilities and limitations of a new thermal finite volume model for the evaluation of laser-induced thermo-mechanical retinal damage

Markus Luecking [a,*], Ralf Brinkmann [b,c], Scarlett Ramos [d], Wilhelm Stork [e], Nico Heussner [d]

[a] FZI Research Center for Information Technology Karlsruhe, Haid-und-Neu-Str. 10, 76131 Karlsruhe, Germany
[b] Institute of Biomedical Optics, University of Luebeck, Peter-Monnik-Weg 4, 23562 Luebeck, Germany
[c] Medical Laser Center Luebeck, Peter-Monnik-Weg 4, 23562 Luebeck, Germany
[d] Robert Bosch GmbH, Herrenwiesenweg 24, 71701 Schwieberdingen, Germany
[e] Institute for Information Processing Technologies, Karlsruhe Institute of Technology, Engesserstrasse 5, 76131 Karlsruhe, Germany

ABSTRACT

Many experimental studies focus on the physical damage mechanisms of short-term exposure to laser radiation. In the nanosecond (ns) pulse range, damage in the Retinal Pigment Epithelium (RPE) will most likely occur at threshold levels due to bubble formation at the surface of the absorbing melanosome. The energy uptake of the melanosomes is one key aspect in modeling the bubble formation and damage thresholds. This work presents a thermal finite volume model for the investigation of rising temperatures and the temperature distribution of irradiated melanosomes. The model takes the different geometries and thermal properties of melanosomes into account, such as the heat capacity and thermal conductivity of the heterogeneous absorbing melanosomes and the surrounding tissue. This is the first time the size and shape variations on the melanosomes' thermal behavior are considered. The calculations illustrate the effect of the geometry on the maximum surface temperature of the irradiated melanosome and the impact on the bubble formation threshold. A comparison between the calculated bubble formation thresholds and the RPE cell damage thresholds within a pulse range of 3 to 5000 ns leads to a mean deviation of $\mu = 22\,\mathrm{mJ/cm^2}$ with a standard deviation of $\sigma = 21\,\mathrm{mJ/cm^2}$. The best results are achieved between the simulation and RPE cell damage thresholds for pulse durations close to the thermal confinement time of individual melanosomes.

1. Introduction

Mechanisms where light can damage irradiated tissue need to be understood to increase the potential and safety of laser applications. Between visible and infrared radiation, the strongest absorbing layer in the mammalian eye is the Retinal Pigment Epithelium (RPE), which is between Bruch}s Membrane and the neural layer of the retina. The RPE cell contains many highly pigmented melanosomes of various geometry. Based on a high pigment density, the RPE layer absorbs approximately 50% of the visible light [1].

A schematic cross-section view of the ocular fundus is shown in Fig. 1. Depending on the wavelength, power density and pulse duration, the laser-induced damage mechanisms are divided into photo-chemical, thermal and thermo-mechanical damage mechanisms, as shown in Fig. 2. Photo-chemical damage occurs at pulse durations longer than 1 s and leads to bleaching processes and destruction of chemical bonds of the irradiated tissue [2]. Thermal damage takes place at pulse durations of 1 μs to a few seconds and is based on the denaturation of the irradiated tissue calculated using an Arrhenius-type activation process [3–6]. Decreasing the pulse duration leads to less heat diffusion between the absorbing melanosome and the surrounding tissue, resulting in a heterogeneous energy distribution within the RPE cell. For a pulse duration below 1 μs, the pulse energy remains localized at the absorbing melanosome and generates a surface temperature rise that can be high enough to cause vaporization of its surrounding medium. These absorbing melanosomes are often the origin of small vapor bubbles that can cause mechanical damage of the surrounding tissue. Another thermo-mechanical damage mechanism called photodisruption occurs at a pulse duration below 1 ns at high energy densities, which can lead to the formation of plasma. This plasma can cause shockwaves which mechanically damage the tissue [7]. To understand thermo-mechanical damage during a short time irradiation, knowledge about the heterogeneous temperature field within the RPE cell is important. Experimental approaches to determine temperature changes within a few nanoseconds on the microscopic scale are almost impossible [8]. Computational models can help improve our understanding of the occurring damage mechanisms and might provide a way to interpolate between experimental data. According to this goal, the numerical simulations of this work show the impact of orientation, shape and

* Corresponding author.
E-mail address: luecking@fzi.de (M. Luecking).

https://doi.org/10.1016/j.compbiomed.2020.103835
Received 11 April 2019; Received in revised form 22 May 2020; Accepted 22 May 2020
Available online 25 May 2020

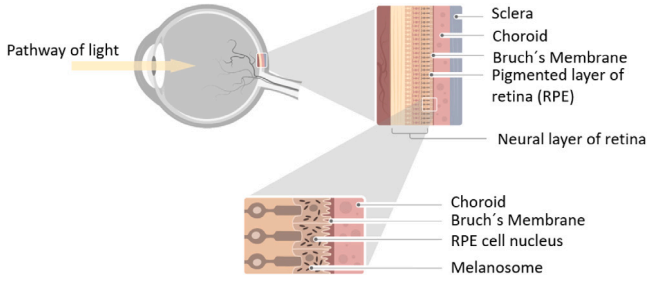

Fig. 1. Anatomy of the human eye.

size differences of irradiated melanosomes on bubble formation and therefore on the thermo-mechanical RPE cell damage threshold.

2. Theoretical background

The nucleation temperature for bubble formation and the bubble dynamics at the irradiated melanosome surface have been the focus of many studies [9–11].

2.1. Bubble formation

The bubble formation around irradiated absorbing tissue at microscale has many unique features and cannot be described by common known nucleation theories [12]. The formation of small bubbles at irradiated melanosomes is not as explosive as an optical breakdown in water because the absorbing material will not evaporate [1,13]. Compared to vaporization by thermodynamic heating, surface tension leads to superheating of the surrounding fluid and high boiling temperatures must be overcome for bubble growth at micrometer scale.

According to Liu et al. [14], the average ellipsoid or spherical melanosome inside a RPE cell has a diameter of 1 µm. The surface pressure is associated with the surface tension σ and the bubble radius r, based on the following equation: $P_{surf} = 2\sigma/r$. Assuming an initial bubble diameter of 1 µm and neglecting the small temperature dependence of the water surface tension, an internal pressure of 3.35 bar is needed to withstand the surface tension. A water pressure of 3.35 bar corresponds to a water temperature of 137 °C, assuming there is thermal equilibrium between the liquid and gas phase. The internal vapor pressure of the bubble must withstand the hydrostatic pressure as well as the surface tension to avoid an unbalanced force equilibrium and an unstable bubble inferface.

The phase transition does not take place in thermal equilibrium and commonly known nucleation theories cannot describe the exact nucleation temperature of the melanosome. Therefore, experimental measurements have been carried out to determine the nucleation temperature. Temperature dependent bubble formation thresholds are often used to determine the nucleation temperature [12]. To determine the nucleation temperature, a water bath with individual melanosomes was heated and the melanosomes were irradiated at different temperatures. The relationship between melanosome temperature and bubble formation threshold for a pulse duration of 12 ns is shown in Fig. 3.

Experimental measurements [12] illustrate the trend of decreasing bubble formation threshold as a function of increasing melanosome temperature. By extrapolating the fit to the melanosome temperature axis (zero input irradiation) the nucleation temperature was determined, as shown in Fig. 3. Energy loss from the heat diffusion between the melanosome and its surrounding was not considered. Therefore, experimental results are only valid for pulse durations within the thermal confinement time of irradiated melanosomes. The nucleation temperature of the melanosomes varies from 116 °C to 167 °C as shown in Table 1. These fluctuations can be explained by different detection methods for bubble formation, different absorption

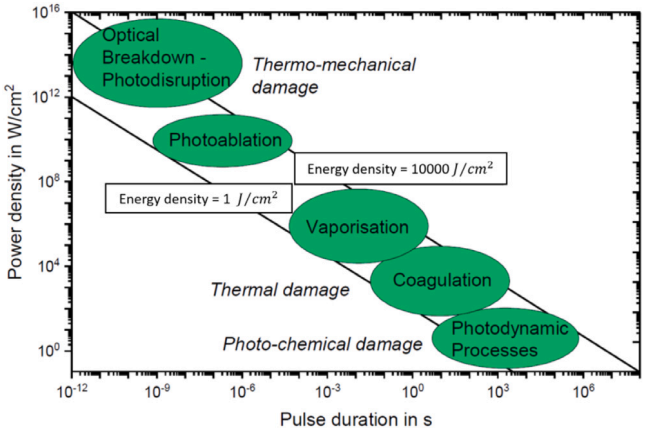

Fig. 2. Laser-induced damage mechanisms [15].

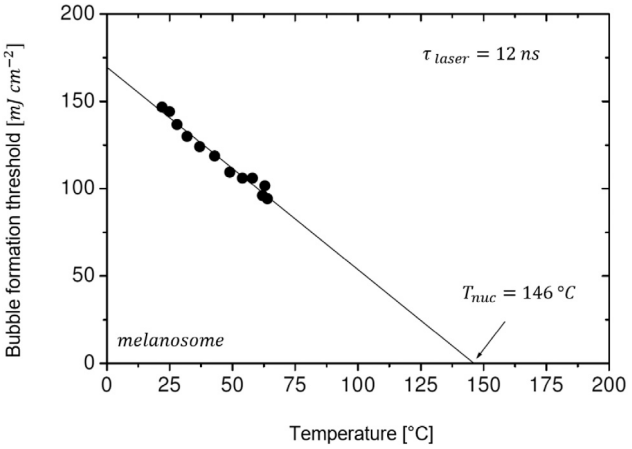

Fig. 3. Temperature dependence of the bubble formation threshold for melanosomes suspended in water, after laser exposure with a wavelength of 532 nm and a pulse duration of 12 ns [12].

Table 1
Nucleation temperatures of RPE melanosomes.

Author	Type	Pulse duration [ns]	Nucleation temperature [°C]
Schmidt [16]	Bovine	10	116
Jacques [17]	Porcine	10	125
Neumann [12]	Porcine	12 – 1800	147 ± 20
Brinkmann [1]	Bovine	20	150
Kelly [18]	Bovine	20	150

coefficients (melanization) and surface modifications of the irradiated melanosomes. According to investigations by Neumann et al. [12], geometry or size differences have no significant influence on the nucleation temperature. For our thermal calculations, a nucleation temperature of 150 °C was used. This nucleation temperature has been measured in different studies [1,18] and is high enough to overcome the surface tension at a melanosome with a minimum diameter of 1 µm.

2.2. Absorption coefficient

The absorption coefficient must be known to describe the thermal behavior of irradiated melanosomes. Depending on the measurement method, model assumptions, irradiated tissue, water content and melanization level, different RPE melanosome absorption coefficients have been obtained. The value of the absorption coefficient varies from 2300 cm^{-1} to 16 000 cm^{-1}, as presented in Tables 2–5.

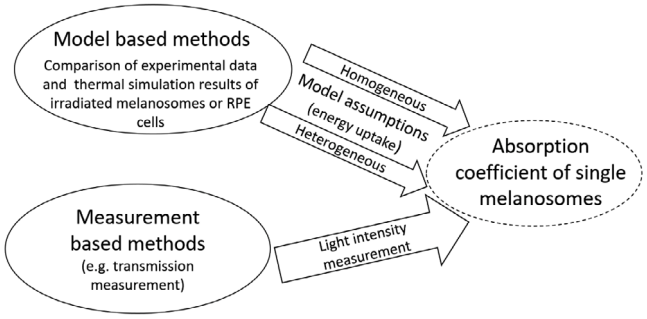

Fig. 4. Sketch of the absorption coefficient determination.

Table 2
Absorption coefficients of RPE melanosomes, determined from transmission measurements.

Author	Type	T_{nuc} [°C]	μ_{abs} [cm^{-1}]
Williams [19]	Mouse	–	9000 – 11 000
Gabel [20]	Human	–	16 000

Table 3
Absorption coefficients of RPE melanosomes, determined from temperature dependent bubble formation thresholds.

Author	Type	T_{nuc} [°C]	μ_{abs} [cm^{-1}]
Jacques [17]	Bovine	125	2300
Schmidt [16]	Bovine	116	3484
Neumann [12]	Porcine	147	5300
Brinkmann [1]	Bovine	150	9900

Fig. 4 shows different methods to determine the absorption coefficient from experimental measurements. The absorption coefficients of melanosomes can be determined directly (e.g. from transmission measurements) or indirectly (e.g. experimental bubble formation) by comparing experimental data with the thermal simulation results of irradiated individual melanosomes. The results of the thermal simulation are derived from analytical models of individual melanosomes and depend on the model assumptions made (e.g. homogeneous or heterogeneous energy uptake). Assuming the material properties of the melanosome and its nucleation temperature are known, the absorption coefficient of the individual melanosome can be determined as the only free model parameter by comparing experimental data and simulation results.

Regarding the absorption coefficients, direct optical transmission measurements on individual melanosomes and RPE cells were carried out by Williams et al. [19] and Gabel et al. [20]. Here, an influence on the absorption measurement by a change of the optical properties due to the preparation process cannot be completely excluded. Therefore, those absorption coefficients were not selected in this study.

Schmidt et al. [16], Neumann et al. [12], Jacques et al. [17] as well as Brinkmann et al. [1] have determined the absorption coefficient of RPE melanosomes by measuring the laser-induced bubble formation threshold at different melanosome temperatures. Because of their assumption of a linear relationship between the melanosome temperature and the bubble formation threshold, absorption coefficients were not considered in this study. Note that the evaporation enthalpy of the surrounding water would lead to a non-linear relationship between the melanosome temperature and the bubble formation threshold at a higher temperature.

Schulmeister et al. [4] were able to fit Ex Vivo cell damage thresholds with his thermal simulation results assuming a spherical melanosome with a diameter of 0.8 µm and a center to center distance of 1 µm. However, melanosomes are not homogeneously distributed within the RPE cell and the calculated absorption coefficient might not be correct.

Table 4
Absorption coefficients of RPE melanosomes, determined from RPE cell damage thresholds.

Author	Type	T_{nuc} [°C]	μ_{abs} [cm^{-1}]
Schulmeister [4]	Bovine	–	00

Table 5
Absorption coefficients of RPE melanosomes, determined from pulse duration dependent bubble formation thresholds.

Author	Type	T_{nuc} [°C]	μ_{abs} [cm^{-1}]
Neumann [12]	Porcine	–	8300
Brinkmann [1]	Bovine	–	8000

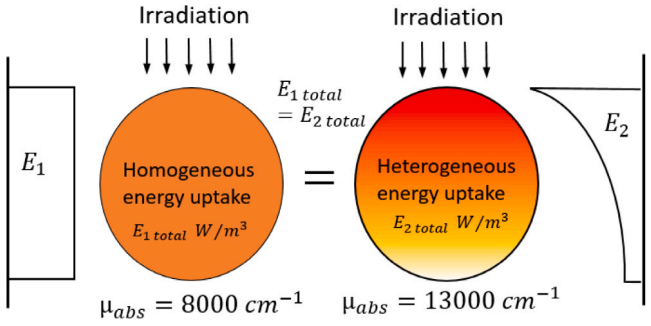

Fig. 5. Sketch of the homogeneous and heterogeneous energy uptake at spherical absorbers.

Neumann et al. [12] and Brinkmann et al. [1] also determined the absorption coefficients by comparing the experimental bubble formation thresholds for different pulse durations with an analytical thermal model, assuming a constant nucleation temperature of 147 °C and 150 °C, respectively. The absorption coefficient was calculated under the assumption of homogeneous energy uptake within the irradiated spherical melanosome.

The assumption of a homogeneous energy uptake cannot be correct for all pulse durations. There is not enough time for heat diffusion to compensate the temperature differences within the melanosome if the pulse duration is below the thermal confinement time of the irradiated melanosome. Temperature differences are based on the fact that the front surface of the irradiated melanosome is exposed to a higher intensity than the back surface. Since Kelly [18] and Brinkmann et al. [1] independently determined a nucleation temperature of 150 °C for bovine RPE melanosomes, the absorption coefficient of 8000 cm^{-1} determined by Brinkmann et al. [1] was chosen. Assuming a constant total energy uptake, the homogeneous energy uptake within the melanosome with an absorption coefficient of 8000 cm^{-1} is equal to a heterogeneous energy uptake with an absorption coefficient of 13 000 cm^{-1}, as illustrated in Fig. 5 [1]. To consider the heterogeneous energy uptake at irradiated melanosomes, we used in our simulations an absorption coefficient of 13 000 cm^{-1}.

2.3. Bubble dynamics

Microbubbles of several micrometers diameter were observed around irradiated melanosomes using short time photography [21]. For a more precise characterization of bubble dynamics, additional interferometric and optoacoustic measurements on irradiated individual melanosomes were carried out [10,22,23].

Interferometric measurements showed clear bubble formation thresholds for individual melanosomes, as presented in Fig. 6. The bubble formation threshold remains approximately constant for multiple irradiations, at a laser pulse duration of 240 ns. This result indicates reproducible nucleation conditions at individual melanosomes, whereas

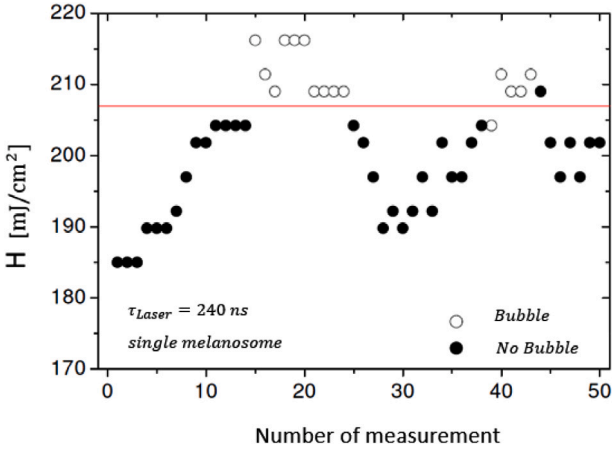

Fig. 6. Bubble formation thresholds during multiple irradiation of the same melanosome with a single pulse duration of 240 ns [12].

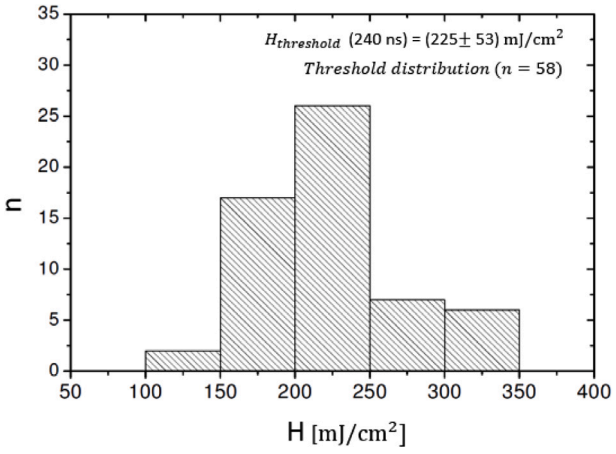

Fig. 7. Threshold distribution for bubble formation obtained from different melanosomes (n=58) [12].

the bubble formation threshold between different melanosomes showed higher variation, as shown in Fig. 7.

For melanosomes of the same animal type, same pulse duration and same measurement technique, a mean threshold of 225 mJ/cm^2 with a standard deviation of 53 mJ/cm^2 could be determined. According to Neumann et al. [24], the threshold variation between individual melanosomes can be caused by a different shape, size, orientation and absorption coefficient.

2.4. Thermo-mechanical damage

Thermo-mechanical damage is often associated with the appearance of microbubbles. Cell damage can be caused by an overstretching of the RPE cell membrane because of intracellular bubble formation. The overstretching of the cell membrane is based on bubble growth within the irradiated RPE cell. The internal bubble growth is determined by the number of bubbles on individual melanosomes, as shown in Fig. 8. A model from Neumann et al. [25] showed that bubble diameters required for RPE cell surface expansion decrease as the number of intracellular bubbles increase. According to Needham et al. [26] a relative membrane area increase (ΔA/A) of 4% (at minimum) can trigger cell death. Considering that one RPE cell can contain over 100 melanosomes, which would most likely lead to the same number of bubbles when irradiated suprathreshold, a single bubble radius of $R_b = 0.75\,\mu m$ can cause RPE cell death. A high density of melanosomes

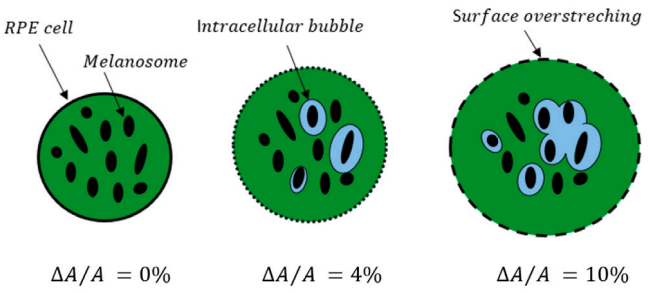

Fig. 8. Sketch of internal bubble growth.

per each RPE cell and a high initial bubble expansion speed of 10 m s^{-1} up to 85 m s^{-1} might cause the coalescence of bubbles around individual melanosomes. Previous studies [10,27] demonstrated that bubble coalescent around individual melanosomes to larger bubbles with a formation time up to a few tens of µs. Therefore, RPE cell death due to thermo-mechanical damage is most likely to occur for short time exposure [9].

2.5. Modeling approaches

In the late 1960s, Hansen and Fine [28] developed a discretized absorption model, based on a uniformly heated, isolated spherical melanosome. The rise of the melanosome temperature was calculated analytically using the heat diffusion equation. In their model, a fixed threshold surface temperature of 100 °C was used to identify the transition from purely thermal and thermo-mechanical damage of irradiated melanosomes. Using this analytical melanosome model, Thompson et al. [29] calculated the retinal temperature rise as the superposition of the thermal contributions of multiple melanosomes. The authors coupled temperature rise to an Arrhenius thermal damage model while assuming cell death for a melanosome surface temperature of 374 °C.

Melanosomes are expected to act as bubble nucleation seeds. Therefore, Gerstman et al. [30] inspected the nucleation condition at the irradiated melanosome. They showed that the bubble formation occurred at lower incident irradiance than required for thermal denaturation for a pulse duration between 1 µs and 1 ns. A detailed theoretical study of Pustovalov et al. [31] showed that the true nucleation condition for the bubble formation around irradiated micro-absorbers is highly complex, including many coupled differential equations and considerations of the coupled physical effects of bubble formation and dynamics.

To the author's knowledge, the influence of shape, size and orientation on bubble formation and thermo-mechanical damage has not been considered in all theoretical models.

3. Model description

This section describes the energy equation for the temperature calculation of an irradiated melanosome, as well as the chosen model parameters and assumptions. The developed three-dimensional models are based on the following heat diffusion equation:

$$\frac{\delta T}{\delta t} = \kappa \nabla^2 T + \frac{Q}{\rho\, c_p} \tag{1}$$

Eq. (1) is solved using the finite-volume-method. Therefore, the heat diffusion in Eq. (1) is temporally and spatially discretized, defining linear equations at each time step whose unknowns are the temperatures of each finite volume. The linear system is solved according to an iterative method using *Ansys Fluent*, a commercial finite-volume-method based solver. The irradiated melanosomes are modeled as absorbers, which are surrounded by a transparent medium. The thermal properties of the absorbing melanosome and the transparent surrounding medium are shown in Table 6.

Table 6
Thermal properties of the absorbing melanosome and the surrounding at $T = 20$ °C [10].

	ρ [kg/m^3]	c_p [J kg^{-1} K^{-1}]	κ [m^2/s]
Melanosome	1400	2250	1.40×10^7
Water	998	4180	1.43×10^7

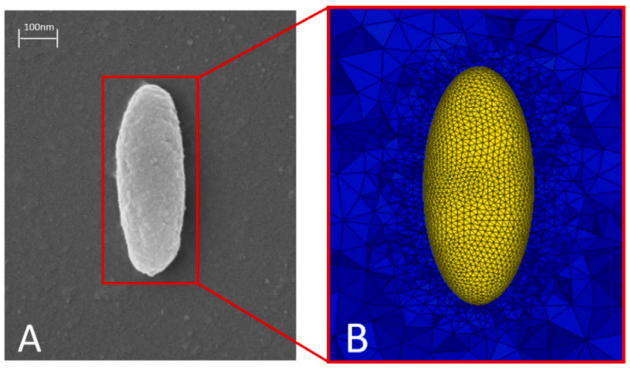

Fig. 9. (A) SEM image of an extracted RPE melanosome; (B) Cross section of the meshed calculation domain.

The thermal properties, ρ as density, c_p as specific heat capacity and k as the thermal diffusivity of Eq. (1) were assumed to be constant at a pressure of 0.1 MPa within a temperature range of 20–150 °C [8]. In all simulations, a constant ambient pressure was assumed.

The energy uptake has a high impact on the temperature evolution because of low heat dissipation, especially for exposure times in the range of ns. In the used heat diffusion equation (1), the input power density of each finite volume per time step is represented as Q [W/m^3]. Power density depends on the absorption within the melanosome and is based on the Beer–Lambert law, as shown in Eq. (2).

$$I(x) = I_0 \cdot e^{-\mu x} \tag{2}$$

In Eq. (2), I_0 represents the intensity [W/m^2], μ the absorption coefficient [m^{-1}] while x represents the path length of the absorbed light [m]. There is not enough time for heat diffusion to compensate the temperature differences within the melanosome for a pulse duration below the confinement time of irradiated melanosome. Temperature differences are based on the fact that the front surface of the irradiated melanosome is exposed to a higher intensity than the back. Therefore, heterogeneous absorption of the melanosome for short time pulse duration was considered, using the so-called *user-defined-function* (UDF) within *Ansys Fluent*. The laser beam profile for all calculations was assumed to be a top-hat due to the small size of the irradiated melanosomes.

For a very close representation of the different melanosome geometries, an elliptically shaped melanosome of different size, was used in this work, as shown in Fig. 9. Compared to numerical methods, analytical approaches have the advantage of increased computational speed. In previous analytical models [1,29] the temperature increase of irradiated melanosomes could only be modeled for a spherical melanosome. To model the thermal influence of the shape and orientation of melanosomes, numerical methods such as the finite-volume-method must be used. Scanning electron microscope (SEM) images of extracted melanosomes showed geometrical variations between individual melanosomes, depending on the tissue origin and their age [14].

The discretization of the elliptical melanosome was performed by *Hypermesh (Altair, Inc)*. Due to the small size of the absorber, tetrahedral finite volume elements were used for meshing. Considering the aim of the present study, a very fine mesh is employed at the interface between the melanosome and the surrounding, allowing for precise control of the temperature change between the two areas.

Table 7
A grid independence study for a pulse duration of 1 ns and time step of 10^{-14} ns.

No. of elements	T_{max} [°C]	ΔT [°C]	Error %
532 532	314.22	–	–
260 421	314.28	0.06	0.02
109 392	319.38	5.16	1.64

Table 8
A time step independence study for a pulse duration of 1 ns.

Time step [s]	T_{max} [°C]	ΔT [°C]	Error %
10^{-13}	314.26	–	–
10^{-12}	314.29	0.03	0.01
10^{-11}	318.32	4.06	1.29
10^{-10}	327.56	13.3	4.23

A grid independence study was carried out for the irradiated melanosome, starting with a fine meshed computational model of 532 547 finite volume cells. The error in maximum melanosome temperature when reducing the number of cells, is shown in Table 7.

Based on the results shown above, a calculation domain with 260 421 cells was selected for an ellipsoid melanosome with the dimension of $1 \times 2.5 \times 1$ µm to avoid large numerical errors. In addition, a suitable time step for the simulations was determined with a time independence study, as shown in Table 8. A starting value a time step of 10^{-13} s was chosen to save computing time.

Table 8 shows that the error in maximum temperature rises with increasing time-steps. To save computational time, a maximum permissible time step of 10^{-12} s was chosen. For all calculations, the following initial and boundary conditions were used:

Initial conditions:

$$T(x,0) = 20\ °C; \quad \text{everywhere}$$

Boundary conditions:

$$T(x,0) = 20\ °C; \quad \text{outer walls}$$

$$\frac{\delta(x,t)}{\delta r} = 0; \quad \text{outer walls.}$$

It should be noted, that the presented model does not include optical effects to consider the scattering or refraction of the irradiated melanosomes. However, according to different studies [32,33], the scattering effects of irradiated melanin or melanosome should not be completely neglected. Sardar et al. [33] applied a conventional method of minimum deviation using a hollow quartz prism to measure the refractive index of single melanin particles. Based on the measured refractive index, they showed that the scattering coefficients are much higher than the absorption coefficient of extracted melanin. How the sample preparation affects the optical behavior of melanin, and how the results could be transferred to describe the optical behavior of irradiated melanosome, could not be clarified within their investigations.

The optical behavior of irradiated melanosomes was the subject of numerical investigations by Song et al. [32]. They simulated the wavelength-dependent optical properties of individual melanosomes, considering their spheroidal geometry, size distribution and complex refraction index. Based on their results, the scattering coefficient of an individual melanosome is at least one order of magnitude higher than the absorption coefficient. It should be noted that the complex refraction index was determined numerically. Information regarding the parameter accuracy of the used complex refraction index are not provided.

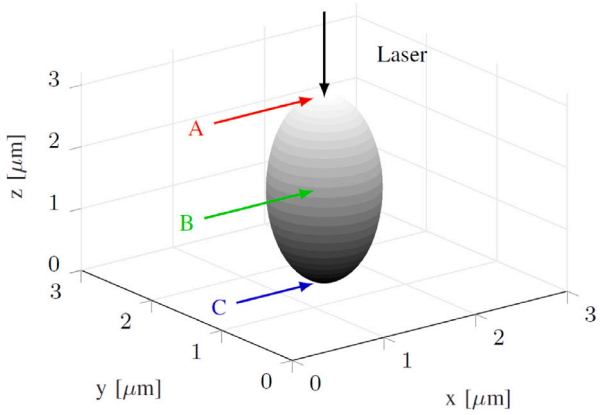

Fig. 10. Sketch of the irradiated melanosome with its long axis parallel to the laser source.

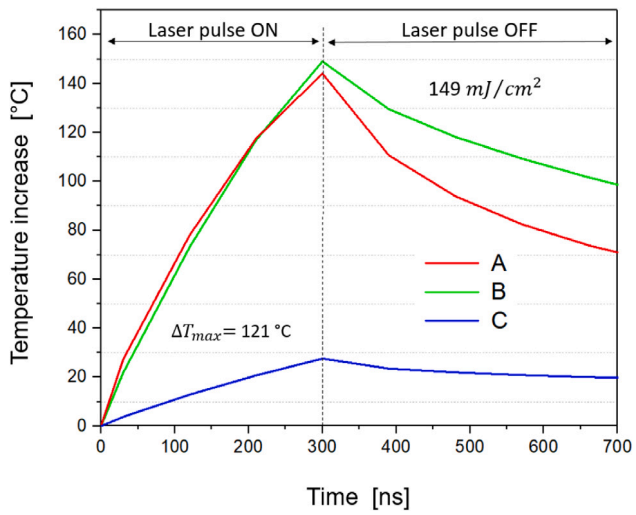

Fig. 11. Surface temperature evolution at different locations on the elliptical melanosome with its long axis parallel to the laser source.

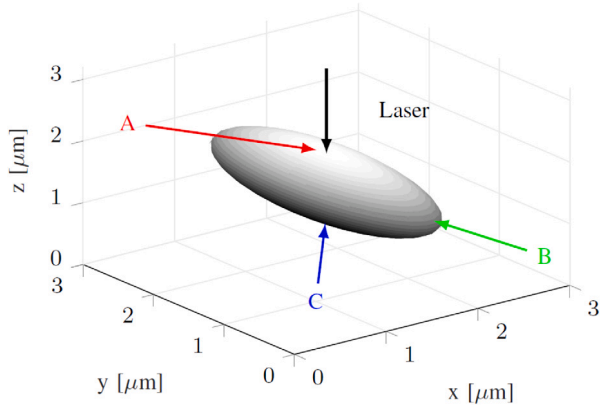

Fig. 12. Sketch of the irradiated melanosome with its long axis perpendicular to the laser source.

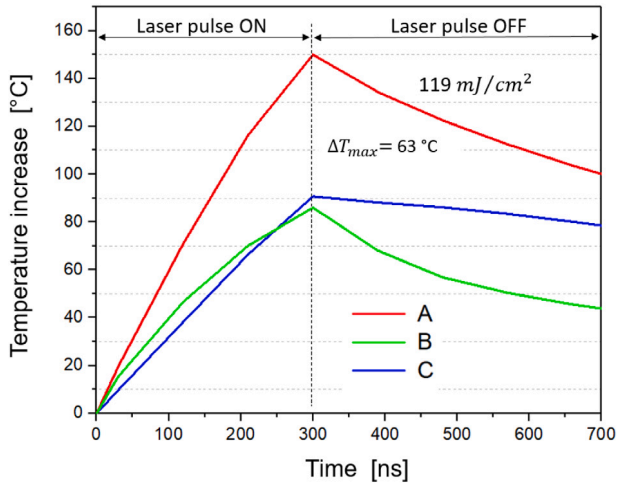

Fig. 13. Surface temperature evolution at different locations on the elliptical melanosome with its long axis perpendicular to the laser source.

4. Results and discussion

This section presents the impact of orientation, size and shape variations on the melanosome temperature for single laser pulse durations from 1 ns to 5 μs.

4.1. Orientation variations

The melanosomes are randomly distributed and orientated within the RPE cell [14]. For this reason, the thermal effect of varying orientations towards the laser source on the melanosome was calculated in this study.

Exemplary calculations for a typical elliptical melanosome (long axis 2.5 μm, short axis 1 μm, aspect ratio 2.5) and a pulse duration of 300 ns were carried out. To determine the temperature gradients on the melanosome surface, the surface temperature of the melanosome was determined at different points. As shown in Fig. 10, the irradiation is parallel to the long axis of the melanosome. The temperature evolution of the melanosome surface at three points are presented in Fig. 11. The highest temperature difference of around 121 °C was calculated after a pulse duration of 300 ns and determined between the indicated points B and C. During the irradiation, the heat diffuses within the melanosome from top to bottom. The surface temperature of point B is therefore affected by the internal heat diffusion. After a pulse duration of 200 ns, the surface temperature of point B is higher than the temperature at point A, the top of the melanosome. The longer diffusion length within the melanosome leads to a lower temperature rise at point C, compared to point B. To evaluate the influence of different orientations, the surface temperature at the points A, B and C were also determined for a melanosome oriented perpendicular to irradiation, as shown in Fig. 12. In comparison with the previous melanosome orientation, smaller temperature gradients could be observed as presented in Fig. 13. A temperature difference of 63 °C at the end of the pulse duration was calculated between point A and B. The heat has to pass a shorter distance to affect the non-irradiated surface of the melanosome, leading to a more homogeneous temperature distribution.

Assuming bubble formation at a melanosome surface temperature of 150 °C, a lower bubble formation threshold could be calculated for melanosomes with a perpendicular orientation. The threshold varies from 117 mJ/cm^2 for the melanosome with perpendicular orientation to 147 mJ/cm^2 for the melanosome with parallel orientation. For the perpendicular orientated melanosome, more surface area with a lower absorption length is irradiated, leading to an improved energy uptake and a reduced threshold value.

4.2. Shape variations

The examination of SEM images of extracted RPE melanosomes showed heterogeneous shaped elliptical melanosomes. These variations

Table 9
Influence of aspect ratio on bubble formation threshold [mJ/cm^2] for different pulse durations, parallel orientation.

Pulse duration [ns]	Threshold [mJ/cm^2]		
	Aspect ratio (a/b)		
	2.0	2.5	3.0
1	86.3	86.64	86.61
5000	632.2	637.3	639.5

Table 10
Influence of aspect ratio on bubble formation threshold [mJ/cm^2] for different pulse durations, perpendicular orientation.

Pulse duration [ns]	Threshold [mJ/cm^2]		
	Aspect ratio (a/b)		
	2.0	2.5	3.0
1	86.2	85.9	85.7
5000	466.1	425.1	386.7

could impact the maximum surface temperature and the bubble formation threshold. The shape of the melanosome is determined by the aspect ratio, defined as the ratio of the long axis to the short axis. In all models the short axis of the elliptical melanosomes is set to 1 μm, whereas the long axis varied from 2.0 μm to 3.0 μm, based on histograms of extracted melanosomes [14].

Calculations were made for two pulse durations and different orientations. The results for a melanosome with the long axis aligned parallel to the laser source are shown in Table 9. For a pulse duration of 1 ns, the threshold results show no significant changes between the different models. A short pulse duration of 1 ns leads to a high heating rate. This heating rate is mainly affecting a thin upper layer of the irradiated melanosome, neglecting temperature changes due to heat diffusion. In this case, the maximum surface temperature is almost independent of the shape of the irradiated absorber. Heat diffusion occurs and the threshold values increase with the size of the longitudinal axis at a pulse duration of 5000 ns. It is assumed that a thermal equilibrium is already reached and the size of the irradiated melanosome has no significant influence on its temperature behavior at a pulse duration of 5000 ns. The temperature distribution after a pulse duration of 1 ns and 5000 ns for a melanosome with an aspect ratio of 2.5 and parallel orientation is shown in Fig. 14.

Changing the orientation changes the absorption length of the elliptical melanosome. Table 10 shows the calculated bubble formation thresholds of a perpendicular orientated melanosome. Similar to the previous results, the results from Table 10 show no threshold differences for a pulse duration of 1 ns. During an irradiation time of 5000 ns, there is an increased heat loss at the tips of the melanosome. The smaller the elliptical melanosome, the greater the effect of the heat loss of the melanosome tips on its core temperature. For long pulse durations, a decreasing core temperature leads to increasing bubble formation threshold. The temperature distribution for an individual melanosome with an aspect ratio of 2.5 and perpendicular orientation is shown in Fig. 15.

4.3. Comparison with experimental bubble formation thresholds

Experimental data shows a large variation of the bubble formation threshold between individual melanosomes. Those measurement results are compared with our calculations on individual RPE melanosomes. Calculations were carried out for an elliptical and a spherical melanosome. In addition, the orientation of the melanosome to the laser source has been changed. Calculation results and experimental data are presented in Fig. 16. Due to high heating rates and negligible heat diffusion, the results show similar threshold values for both shapes and both orientations at a pulse duration of 12 ns.

The threshold values of the presented models differ for longer pulse durations. At a pulse duration of 240 ns, the lowest bubble formation threshold is calculated for an elliptical melanosome, whose long axis is perpendicular to the laser source. Compared to the parallel orientation, the elliptical melanosome with perpendicular orientation has a smaller effective absorption diameter and thus a higher energy uptake. In comparison, the effective absorption diameter of the spherical and the perpendicular aligned elliptical melanosome are identical. The lower thresholds of the elliptical melanosome are based on a higher energy uptake for the same effective absorption diameter since more heat from the upper region diffuses towards the center of the irradiated elliptical melanosome.

The comparison of the thresholds of individual melanosomes at a pulse duration of 240 ns and 585 ns shows that, because of the heat diffusion, higher irradiation is necessary to achieve a nucleation surface temperature of 150 °C. The increased heat diffusion at 585 ns leads to threshold differences between the three melanosome models based on their different absorption length and volume.

4.4. Comparison with experimental RPE cell damage thresholds

Many studies [9,21,23] show a relationship between the detection of microbubbles and the RPE cell death of an irradiated explant. Therefore, Fig. 17 shows Ex Vivo RPE cell thresholds and calculated bubble formation thresholds of the different melanosome models, assuming a bubble formation at 150 °C melanosome surface temperature.

The discrepancy between the RPE damage values and the thermal bubble formation threshold values vary for the different pulse durations, as illustrated in Fig. 17. The RPE cell thresholds are limited to Ex Vivo experiments since those measurements are not affected by any delayed cell damage mechanism (Apoptosis). In Vivo experiments showed that the cell damage after irradiation can deviate from the cell damage after 24 h. The presented thermal model determines the melanosome surface temperature that can lead to bubble formation and cannot represent any time-delayed damage mechanism. To compare the calculated threshold values with existing In Vivo thresholds, the retinal laser radiation must be known. Since the laser beam is passing through various individual media of the eye, the retinal radiation is influenced by various factors. The radiation is affected by the accommodation state of the eye, laser divergence, animal species and the transmission of the laser beam through the individual media of the eye [34]. Based on a large number of unknown influencing factors, a comparison of the calculated bubble formation thresholds with In Vivo thresholds has not been considered.

A large difference between the thermal simulation results and the available RPE cell damage thresholds from Payne et al. [35] can be observed. This discrepancy at a pulse duration of 3 ns might be related to transient pressure reduction of the surrounding and thus affect the nucleation conditions at the melanosome. Based on unknown thermoelastic properties of the melanosome (e.g. grueneisenparameter), the exact pressure cannot be calculated. Thus, further experimental investigation to determine thermoelastic properties of the RPE melanosome, the dependency of the pulse duration as well as nucleation temperature are needed. In addition, it should be considered that short pulses induce a higher bulk temperature of the melanosome or its single melanin particles. This high temperature might lead to a release of the bounded water within the melanin and cause the formation of microbubbles within the melanosome [36]. The thermal stability of ocular melanin pigments and the amount of released water is not exactly known and further experimental measurements are needed to gain a better understanding of the microbubble formation within the melanosome.

Within a pulse range of about 8 ns to 500 ns, there is a better agreement between the shown cell damage thresholds and the simulation results, e.g. comparing the experimental data from Roegener et al. [37] or Brinkmann et al. [1] with the numerical results. The best agreement could be determined for an elliptical melanosome

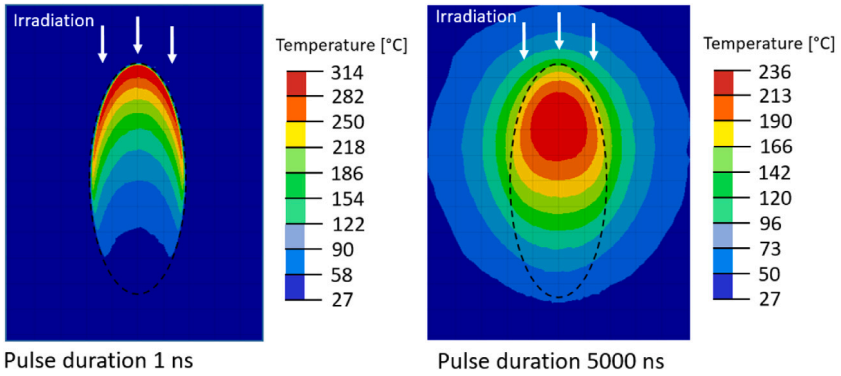

Fig. 14. Temperature profile of the irradiated melanosome with its long axis parallel to the laser source after different pulse durations.

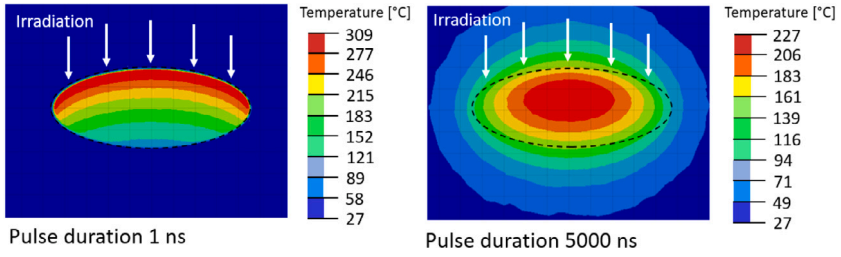

Fig. 15. Temperature profile of the irradiated melanosome with its long axis perpendicular to the laser source after different pulse durations.

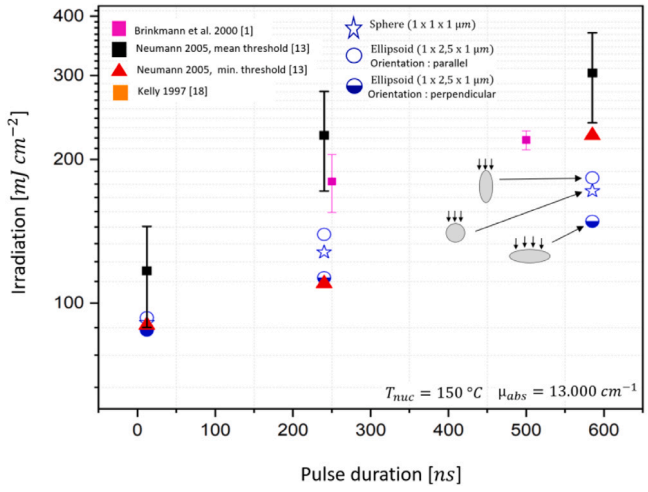

Fig. 16. Threshold radiant exposures for different pulse durations for calculated bubble formation around individual melanosomes and experimental bubble formation thresholds.

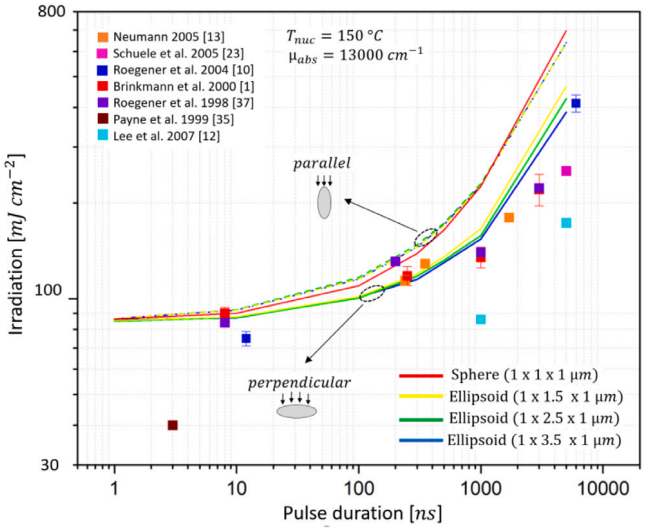

Fig. 17. Threshold radiant exposures as a function of pulse duration for calculated bubble formation around individual melanosomes (solid and dotted line) and experimental ED50 damage thresholds of Ex Vivo RPE cells (squares) from different animals.

(1 μm × 3.0 μm × 1 μm) with a perpendicular orientation. Compared to the spherical melanosome with a diameter of 1 μm, the elliptical melanosome has a larger absorbing volume and thus a lower bubble formation threshold. The differences between those numerical models show the importance of absorber geometry and orientation to the accuracy of the model. Compared to analytical thermal melanosome models [1,29], the strength of the presented numerical models is that the three-dimensional melanosome geometry is covered, achieving a lower discrepancy between the experimental and calculated data. The low discrepancy between the numerical and experimental data could be based on a realistic nucleation temperature and the assumption that the bubble formation on the melanosome surface leads to RPE cell death.

Above 500 ns, there is an increasing discrepancy between the numerical and available experimental results. This discrepancy might be related to the heat diffusion between the absorbing melanosome and its surrounding. To evaluate the thermal impact of surrounding melanosome on the threshold, Fig. 18 presents the calculated threshold of an individual melanosome and a melanosome cluster. The cluster consists of nine individual elliptical melanosomes (1 μm × 2.5 μm × 1 μm) arranged in a formation of 3 × 3 with a random distance to each other of 0.1 μm. As shown in Fig. 18, the threshold difference between the two models whose long axis is perpendicular to the laser source, is increasing at higher pulse durations. Although the distance between the individual melanosome in the cluster is very small, there is no threshold difference between the models for a pulse duration of 1 ns. With increasing pulse duration and thus increasing heat diffusion, the thermal interaction between the clustered melanosome leads to a lower

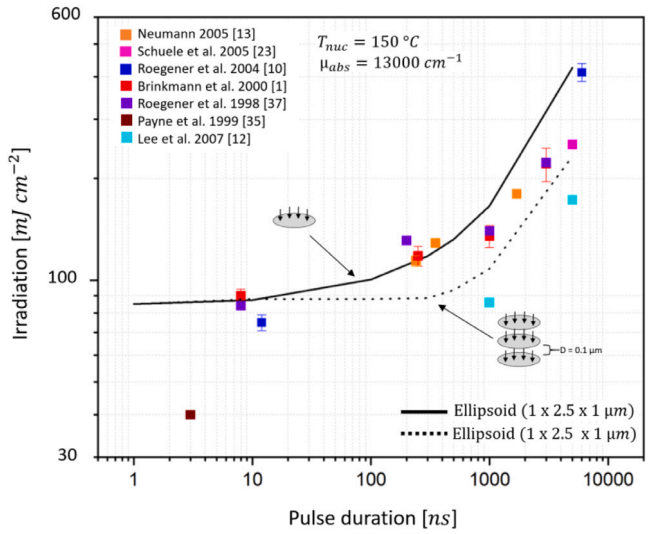

Fig. 18. Threshold radiant exposures as a function of pulse duration for calculated bubble formation around individual as well as clustered melanosomes (solid and dotted line) and experimental ED50 damage thresholds of Ex Vivo RPE cells (squares) from different animals.

heat loss and a lower threshold. From Fig. 18, it is assumed that for the chosen model settings, the thermal interaction between individual melanosomes becomes important above 100 ns. Therefore, considering the thermal interaction between individual melanosomes could lead to a better agreement between the simulation results and the experimental data.

With regard to the comparison between the calculated and experimental thresholds, it should be noted that homogeneous irradiation was assumed in all simulations. However, in many experiments the used beam profile shows fluctuations, leading to a high discrepancy between the mean and peak laser power. Unfortunately, not all publications contain information about the used beam profile, resulting in a more difficult comparison of calculated and experimental thresholds.

5. Conclusion and outlook

The presented results are indicate that, depending on the pulse duration, the surface temperature of irradiated melanosomes is affected by different shapes and orientations. A smaller pulse duration will result in a smaller influence of the geometry and orientation on the temperature profile of the irradiated melanosome. For a pulse duration of 300 ns, the orientation of an elliptical melanosome leads to a threshold difference of 30 mJ/cm^2 ($\approx 20\%$).

The calculated bubble formation thresholds of elliptical melanosomes are in the range of the experimental bubble formation thresholds for a pulse duration of 12 ns. Longer pulse durations lead to more heat loss due to heat diffusion, and thus to a greater discrepancy between simulated and experimentally determined threshold values. A comparison between the calculated bubble formation thresholds and the available experimental RPE cell damage thresholds within a pulse duration of 8 ns to 500 ns leads to a maximum discrepancy of 15 mJ/cm^2. For longer pulse durations, the neglection of the thermal interaction between individual melanosomes could lead to the higher discrepancy between the thermal model of an individual melanosome and the experimentally determined threshold data. A short pulse duration of 3 ns leads to a higher discrepancy between the calculated bubble formation thresholds and the experimental RPE cell damage threshold, due to transient pressure reduction of its surrounding and high temperature increase within the melanosome. The nucleation temperature and the absorption coefficient are not necessarily constant for different pulse durations or species, therefore the differences between numerical and experimental results might be related to variations of optical and thermal properties of the irradiated melanosome. The differences between the numerical and experimental results might also indicate that the calculation of the melanosome surface temperature is not sufficient for the exact determination of the thermo-mechanical damage. Therefore, further thermo-mechanical damage mechanisms have to be taken into account for the precise determination of thermo-mechanical damage within the pulse range of a few ns.

As stated in previous sections, scattering effects should be considered for more precise thermal simulations of irradiated melanosomes. Thus, investigations on the complex refraction index of individual melanosomes immersed in water, and numerical simulations of scattering effects of irradiated melanosomes, will be subjects for our future investigations.

References

[1] R. Brinkmann, G. Huettmann, J. Roider, R. Birngruber, C. Lin, Origin of retinal pigment epithelium cell damage by pulsed laser irradiance in the nanosecond to microsecond time regimen, Lasers Surg. Med. 27 (2000) 451–464, http://dx.doi.org/10.1016/0003-4916(63)90068-X.

[2] J. Hunter, J. Morgan, W. Merigan, D. Sliney, J. Sparrow, D. Williams, The susceptibility of the retina to photochemical damage from visible light, Prog. Retin. Eye Res. 31 (2011) 28–42, http://dx.doi.org/10.1016/j.preteyeres.2011.11.001.

[3] N. Heussner, L. Holl, T. Nowak, T. Beuth, M. Spitzer, W. Stork, Prediction of temperature and damage in an irradiated human eye—utilization of a detailed computer model which includes a vectorial blood stream in the choroid, Comput. Biol. Med. 51 (2014) 35–43, http://dx.doi.org/10.1016/j.compbiomed.2014.04.021.

[4] K. Schulmeister, J. Husinsky, B. Seiser, F. Edthofer, B. Fekete, L. Farmer, D. Lund, Ex vivo and computer model study on retinal thermal laser-induced damage in the visible wavelength range, J. Biomed. Opt. 13 (2008) 054038, http://dx.doi.org/10.1117/1.2982526.

[5] N. Heussner, W. Stork, Damage evaluation of the human eye for different laser sources–connecting ray tracing and finite volume calculations, J. Med. Bioeng. 4 (2015) http://dx.doi.org/10.12720/jomb.4.6.475-479.

[6] A. Welch, The thermal response of laser irradiated tissue, IEEE J. Quantum Electron. 20 (12) (1984) 1471–1481, http://dx.doi.org/10.1109/JQE.1984.1072339.

[7] B.A. Rockwell, R.J. Thomas, A. Vogel, Ultrashort laser pulse retinal damage mechanisms and their impact on thresholds, Med. Laser Appl. 25 (2) (2010) 84–92, http://dx.doi.org/10.1016/j.mla.2010.02.002.

[8] J. Neumann, R. Hagenau, G. Schüle, B. Schweda, R. Brinkmann, Finite element calculation of the temperature distribution in a RPE cell during and after μ s-laser exposure, in: Biophotonics: Photonic Solutions for Better Health Care VI, in: Proceedings Laser Bioeffects Meeting, International Commission on Non Ionizing Radiation Protection, 2002, pp. 60–72.

[9] J. Roegener, R. Brinkmann, C.P. Lin, Pump-probe detection of laser-induced microbubble formation in retinal pigment epithelium cells, J. Biomed. Opt. 9 (2) (2004) 367–371, http://dx.doi.org/10.1117/1.1646413.

[10] J. Neumann, R. Brinkmann, Boiling nucleation on melanosomes and microbeads transiently heated by nanosecond and microsecond laser pulses, J. Biomed. Opt. 10 (2) (2005) 1–12, http://dx.doi.org/10.1117/1.1896969.

[11] H. Lee, C. Alt, C.M. Pitsillides, C.P. Lin, Optical detection of intracellular cavitation during selective laser targeting of the retinal pigment epithelium: dependence of cell death mechanism on pulse duration, J. Biomed. Opt. 12 (6) (2007) 1–14, http://dx.doi.org/10.1117/1.2804078.

[12] J. Neumann, Mikroskopische Untersuchungen zur laserinduzierten Blasenbildung und -dynamik an Absorbierenden Mikropartikeln (Ph.D. thesis), Luebeck University, 2005.

[13] J. Sun, B. Gerstman, B. Li, Bubble dynamics and shock waves generated by laser absorption of a photoacoustic sphere, J. Appl. Phys. 88 (2000) 2352–2362, http://dx.doi.org/10.1063/1.1288507.

[14] Y. Liu, L. Hong, K. Wakamatsu, S. Ito, B.B. Adhyaru, C. Cheng, C.R. Bowers, J.D. Simon, Comparisons of the structural and chemical properties of melanosomes isolated from retinal pigment epithelium, Iris and choroid of newborn and mature bovine eyes, Photochem. Photobiol. 81 (3) (2005) 510–516, http://dx.doi.org/10.1562/2004-10-19-RA-345.

[15] S. Ramos, M. Reh, G. Zeck, N. Heussner, Evaluation of short pulse laser damage to the retinal pigment epithelium layer: a key point for the assessment of devices using the nanosecond regime, in: J. Popp, V.V. Tuchin, F.S. Pavone (Eds.), Biophotonics: Photonic Solutions for Better Health Care VI, Vol. 10685, International Society for Optics and Photonics, SPIE, 2018, pp. 60–72, http://dx.doi.org/10.1117/12.2306893.

[16] M.S. Schmidt, P.K. Kennedy, G.D. Noojin, R.J. Thomas, B.A. Rockwell, Temperature dependence of melanosome microcavitation thresholds produced by single nanosecond laser pulses, in: E.D. Jansen (Ed.), Optical Interactions with Tissue and Cells XXVI, Vol. 9321, International Society for Optics and Photonics, SPIE, 2015, pp. 51–58, http://dx.doi.org/10.1117/12.2079934.

[17] S.L. Jacques, R.D. Glickman, J.A. Schwartz, Internal absorption coefficient and threshold for pulsed laser disruption of melanosomes isolated from retinal pigment epithelium, in: S.L. Jacques (Ed.), Laser-Tissue Interaction VII, Vol. 2681, International Society for Optics and Photonics, SPIE, 1996, pp. 468–477, http://dx.doi.org/10.1117/12.239608.

[18] M.W. Kelly, Intracellular Cavitation as a Mechanism of Short-Pulse Laser Injury to the Retinal Pigment Epithelium (Ph.D. thesis), Tufts University, 1997.

[19] M. Williams, L. Pinto, J. Gherson, The retinal pigment epithelium of wild type (c57bl/6j +/+) and pearl mutant (c57bl/6j pe/pe) mice, Investig. Ophthalmol. Vis. Sci. 26 (1985) 657–669.

[20] V.P. Gabel, R. Birngruber, F. Hillenkamp, Visible and near infrared light absorption in pigment epithelium and choroid, in: XXIII Concilium Ophthalmologicum, Vol. 450, 1978, pp. 658–662.

[21] C.P. Lin, M.W. Kelly, S.A.B. Sibayan, M.A. Latina, R.R. Anderson, Selective cell killing by microparticle absorption of pulsed laser radiation, IEEE J. Sel. Top. Quantum Electron. 5 (4) (1999) 963–968, http://dx.doi.org/10.1109/2944.796318.

[22] J. Neumann, R. Brinkmann, Interferometric noncontact on-line dosimetry control during selective retina treatment (SRT), in: Progress in Biomedical Optics and Imaging - Proceedings of SPIE, Vol. 5695, 2005, http://dx.doi.org/10.1117/12.602290.

[23] G. Schuele, M. Rumohr, G. Hüttmann, R. Brinkmann, Rpe damage thresholds and mechanisms for laser exposure in the microsecond-to-millisecond time regimen, Investig. Ophthalmol. Vis. Sci. 46 (2005) 714–719, http://dx.doi.org/10.1167/iovs.04-0136.

[24] J. Neumann, R. Brinkmann, Nucleation dynamics around single microabsorbers in water heated by nanosecond laser irradiation, J. Appl. Phys. 101 (2007) 114701, http://dx.doi.org/10.1063/1.2740348.

[25] J. Neumann, R. Brinkmann, Nucleation and dynamics of bubbles forming around laser heated microabsorbers, in: Progress in Biomedical Optics and Imaging - Proceedings of SPIE, Vol. 5863, 2005, http://dx.doi.org/10.1117/12.633102.

[26] D. Needham, R.S. Nunn, Elastic deformation and failure of lipid bilayer membranes containing cholesterol, Biophys. J. 58 (1990) 997–1009, http://dx.doi.org/10.1016/S0006-3495(90)82444-9.

[27] A. Fritz, L. Ptaszynski, H. Stoehr, R. Brinkmann, Dynamics and detection of laser induced micro bubbles in the retinal pigment epithelium (RPE), in: Progress in Biomedical Optics and Imaging - Proceedings of SPIE, Vol. 6632, 2007, http://dx.doi.org/10.1117/12.728344.

[28] W.P. Hansen, S. Fine, Melanin granule models for pulsed laser induced retinal injury, Appl. Opt. 7 (1) (1968) 155–159, http://dx.doi.org/10.1364/AO.7.000155.

[29] C. Thompson, B. Gerstman, S. Jacques, Melanin granule model for laser-induced thermal damage in the retina, Bull. Math. Biol. 58 (1996) 513–553, http://dx.doi.org/10.1007/BF02460595.

[30] B. Gerstman, C. Thompson, S. Jacques, M. Rogers, Laser-induced bubble formation in the retina, 1995, pp. 60–71, http://dx.doi.org/10.1117/12.209929.

[31] V. Pustovalov, Thermal processes under the action of laser radiation pulse on absorbing granules in heterogeneous biotissues, Int. J. Heat Mass Transfer 36 (1993) 391–399, http://dx.doi.org/10.1016/0017-9310(93)80015-M.

[32] W. Song, L. Zhang, S. Ness, J. Yi, Wavelength-dependent optical properties of melanosomes in retinal pigmented epithelium and their changes with melanin bleaching: A numerical study, Biomed. Opt. Express 8 (2017) 3966, http://dx.doi.org/10.1364/BOE.8.003966.

[33] D.K. Sardar, M.L. Mayo, R.D. Glickman, Optical characterization of melanin, J. Biomed. Opt. 6 (4) (2001) 404–411, http://dx.doi.org/10.1117/1.1411978.

[34] C. Framme, C. Alt, S. Schnell, M.E. Sherwood, R. Brinkmann, C.P. Lin, Selective targeting of the retinal pigment epithelium in rabbit eyes with a scanning laser beam., Investig. Ophthalmol. Vis. Sci. 48 4 (2007) 1782–1792.

[35] D. Payne, T.R. Jost, J.J. Elliot, B. Eilert, L. Lott, K. Lott, G.D. Noojin, R.A. Hopkins, C.P. Lin, B.A. Rockwell, Cavitation thresholds in the rabbit retinal pigmented epithelium, in: S.L. Jacques, G.J. Mueller, A. Roggan, D.H. Sliney, D.H. Sliney, G.J. Mueller, A. Roggan (Eds.), Laser-Tissue Interaction X: Photochemical, Photothermal, and Photomechanical, Vol. 3601, International Society for Optics and Photonics, SPIE, 1999, pp. 27–31, http://dx.doi.org/10.1117/12.350019.

[36] S. Sajjan, A. Oblesha, G. Kulkarni, A. Nayak, T.B. Karegoudar, Properties and functions of melanin pigment from klebsiella sp. GSK, Korean J. Microbiol. Biotechnol. 41 (2012) http://dx.doi.org/10.4014/kjmb.1210.10002.

[37] J. Roegener, Schadensmechanismus bei der Laserbestrahlung des Retinale Pigmentepithels mit Nano- und Mikrosekundenpulsen (Master's thesis), Medizinisches Laserzentrum Luebeck, 1998.

Markus Lücking received his Diploma degree in engineering from the Technical University Braunschweig, Germany. His Diploma thesis focused on the investigation of damage of the lithium-ion batteries. Currently, he is a working as research scientist at FZI Research Center for Information Technology. Subject of his work is the numerical investigation of thermomechanical damage concerning eye safety.

Dr. Ralf Brinkmann studied physics at the University of Hannover, Germany, with a focus on quantum optics and lasers. After a five years industrial interim period he joined the Medical Laser Center in Lübeck, Germany, in 1993, and received his Ph.D. at the University of Lübeck. Since 2005 he holds a permanent position as faculty member at the University Institute of Biomedical Optics, and is also leading the Medical Laser Center Lübeck as CEO.

Scarlett Ramos received her B.Sc. and M.Sc. degrees in biomedical engineering from Stuttgart University, Germany. Her master's thesis focused on the investigation of damage of the retinal pigment epithelium by nanosecond laser irradiation. Currently, she is a Ph.D. student at the Karlsruhe Institute of Technology and at Robert Bosch GmbH. Subject of her Ph.D.thesis is the investigation of thermomechanical damage concerning eye safety for automotive LiDAR.

Prof. Dr. rer. nat. Wilhelm Stork studied physics with a focus on optics and digital image processing at the University of Munich and the University of Erlangen-Nürnberg. Since 1993 he is responsible for the establishment and management of the research area Microsystems Technology and Optics at the University of Karlsruhe at the Institute for Information Processing Technology (ITIV). Author and coauthor of numerous publications focusing on optoelectronic sensor technology in medicine and technology, design methods and computer-aided tools for micro-optical systems and components.

Dr. Nico Heussner studied electrical engineering with a focus on optical technologies at the Karlsruhe Institute of Technology (KIT) and the University of St. Andrews. During his PhD thesis at the FZI Research Center for Information Technology he worked successfully on the modeling of retinal damage. Since 2015 he is responsible for ocular safety of LiDAR devices at Robert Bosch GmbH including research topics which concern with modeling and measurements of thermomechanical damage to the retina.